Methodology to assess phasor measurement unit in the estimation of dynamic line rating

Alvarez, David; Silva, Filipe Miguel Faria da; Bak, Claus Leth; Mombello, Enrique; Rosero, Javier; Ólason, Daníel L.

Published in:
IET Generation, Transmission & Distribution

DOI (link to publication from Publisher):
10.1049/iet-gtd.2017.0661

Publication date:
2018

Document Version
Accepted author manuscript, peer reviewed version

IET Research Journals

Case Studies

ISSN 1751-8644
doi: 0000000000
www.ietdl.org

A Methodology to Assess PMU in the Estimation of Dynamic Line Rating

David L. Alvarez[1], F. Faria da Silva[2], Claus Leth Bak[2], Enrique E. Mombello[3], Javier A. Rosero[1], Daníel Leó Ólason[4]*

[1] *Electrical Machines & Drives Group, EM&D, Universidad Nacional de Colombia, Bogotá, Colombia*
[2] *Department of Energy Technology, Aalborg University, Aalborg, Denmark*
[3] *Instituto de Energía Eléctrica, CONICET, Universidad Nacional de San Juan, San Juan, Argentina*
[4] *LANDSNET, Iceland*
* *E-mail: dlalvareza@unal.edu.co*

Abstract: This paper presents a methodology to analyse the influence of both atmospheric variations in time and space and the error in synchrophasor measurements to estimate conductor temperature along an overhead line. In this methodology, expressions to compute the error propagation in the computing of temperature as a consequence of measurement errors and load variations are proposed. The analysis begins by computing overhead line's thermal and mechanical parameters using simulations of load and atmospheric conditions. The weather in each span is interpolated using nearby weather stations. Having computed thermal and mechanical parameters, values of resistance, inductance and capacitance of the overhead line modelled by means of a π equivalent circuit are estimated, with the purpose of quantifying the sensibility of electrical parameters to changes in conductor temperature. Additionally, this analysis allows the identification of the temperature in each span along OHLs. Subsequently, the average conductor temperature is estimated using simulations of synchrophasors through the relationship between resistivity and temperature. This estimated temperature is compared with the temperature computed using atmospheric conditions in order to obtain the maximum error. This error is contrasted with the acceptable error margins. Thus, during the planning stage, this methodology can be used to assess PMU as a method of computing conductor temperature.

1 Introduction

Power systems are facing new challenges in operation, control and planning. To better face these challenges, it is necessary to optimize assets capacity, because they have reached their limits as a consequence of new loads and sources [1]. These new loads and sources increase congestion and risk, especially in overhead lines (OHLs) [2]. Thus, to push limits in OHLs, new technologies and methods have been developed with the aim of improving their capacity, reliability, safety and economic operation [3]. Among these technologies is Dynamic Line Rating (DLR) which has the ability to compute conductor's ampacity in real time, based on current weather [4]. Rating in medium and short OHLs is commonly determined by catenary sag [5], a limit given by a maximum temperature in the conductor. Hence, DRL is typically used for this kind of OHLs.

Traditionally, line ratings are fixed according to extreme climate conditions that rarely happen. However, thanks to development of information technologies, it is possible to compute online OHL's rating, via measurements of atmospheric conditions and current intensity. Two types of measurements for DLR have been defined, they are called direct and indirect [6]. The indirect method uses weather stations near to the OHLs whereas direct methods uses sensors of mechanical tension, temperature, sag or measurements derived from these three variables. Devices used in direct methods are located directly in the OHL, making it difficult to put them into operation and requiring maintenance. Despite this, DLR has low costs and it is fast to implement, if compared with other methods used to increase OHL's ampacity [7]. Additionally, DLR is useful when it is necessary to increase the capacity between 10% and 30%, particularly for wind power integration [8], given the relationship between wind speed, power generation and cooling. In brief, DLR increases the capacity of OHL most of the time, achieving asset optimization.

The use of PMUs allows the estimation of OHL's conductor thermal capacity in real-time. This method is considered as DLR technology, with the advantage that it uses an existing infrastructure capable of guaranteeing the functioning and reliability of DLR system [9]. With PMU, conductor rating is estimated using impedance of OHL equivalent circuit [10, 11], because of impedance changes according to conductor temperature. This temperature impacts state estimation [12] and load flows [13], thereby affecting losses, bus voltages, protections schemes [14] and OHL ampacity, among others.

The use of PMU for DLR is based on the computing of OHL's average conductor temperature. However, conductor temperature varies along OHL, as a consequence of atmospheric variations in the different spans. Reference [15] presents a methodology for incorporating temperature variations along OHLs. This methodology consists of dividing line in segments based on temperature gradients obtained from measurements along the conductor. In same way, in reference [16] critical spans for monitoring OHLs are estimated by means of weather forecasting models, considering climate variations in time and space. However, there is not literature on the assessment of the error obtained by using resistance to compute OHL's conductor temperature.

This paper proposed a methodology which consists in analysing, through simulations and analytically, the influence of measurement errors and atmospheric variations in time as well as space in the estimation of conductor temperature when PMUs are used. This methodology can be used to assess PMU for computing OHL's conductor temperature. This in order to ensure that the estimated temperature error does not exceed acceptable margins. This paper is organized as follows: Section 2 discusses multiphysics behaviour of OHLs when changes in weather or load occur. In section 3, the proposed expressions to compute error propagation are addressed when synchrophasors are used. Section 4 describes the OHL under study and the interpolation method used to compute atmospheric conditions along an OHL. In section 5, the impact of weather over conductor temperature is computed in each ruling span and compared with the temperature calculated using PMU measurements. Finally, Section 6 analyses the error in estimation both OHL resistance and temperature when PMU measurements are used, taking into account measurement accuracy and load variations.

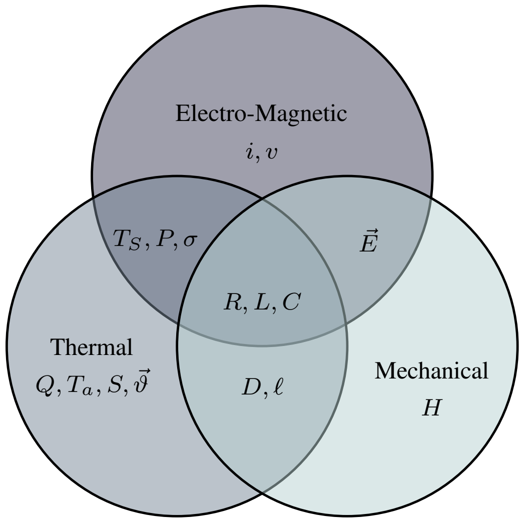

Fig. 1: Multiphysical phenomena in OHLs as a result of heat transfer

2 Multiphysics Phenomena - Background

During operation, OHLs are under influence of thermal, mechanical and electrical phenomena [17]. Figure 1 shows the relationship between these physical phenomena. At first, a heat transfer (Q) is presented as a product of a heat gain (mainly by Joule effect (P) and solar radiation (S)) and a heat loss (radiation and convection). That heat transfer is determined by the current intensity $|i_{km}|$, conductor properties and by atmospheric conditions (ambient temperature (T_a), solar radiation, and wind speed and direction $\left(\vec{\vartheta}\right)$). Heat transfer affects the conductor temperature (T_S), leading to a variation in the horizontal component of conductor mechanical tension (H), as a result of changes in conductor length (ℓ) and in catenary sag (D). Additionally, changes in T_S, D, ℓ impact both electric field $\left(\vec{E}\right)$ distribution and conductor electrical conductivity (σ). These variations reflect in the values of voltage (v) and current intensity (i) in OHL's. Finally, these three physical phenomena affect the OHL's RLC parameters, given that these parameters depend on line geometry and conductor properties.

2.1 *Thermal phenomena*

CIGRE [18] and IEEE [19] standards are commonly used for computing temperature in OHL conductors. These standards are based on the heat balance equation. For thermal steady state, eq. (1) is used,

$$Q_J + Q_S = Q_C + Q_R \tag{1}$$

where Q_J is the heat gain from the Joule effect, Q_S is the gain from solar radiation, Q_C is the loss for convective cooling and Q_R is the loss for radiative cooling. The gain from magnetic heating and corona heating, as well as the losses due to evaporative cooling, are commonly ignored.

From eq. (1), the conductor temperature T_S and the maximum current intensity can be computed, provided that atmospheric conditions, current intensity and conductor properties (resistivity, temperature coefficient of resistance, solar absorptivity of surface, solar emissivity of surface, diameter, among others) are known.

2.2 *Mechanical phenomena*

Temperature variations in conductors result in changes in their length and on forces that act on catenary. To model this behavior, numerical or analytic formulations can use. Numerical methods such as Finite Elements are not commonly used for DLR, because of they require specialized software and large computational resources when compared with analytical approximations. As an analytical method, the state change equation (2) approximates the mechanical tension in an OHL stringing section using the ruling span method [20, 21].

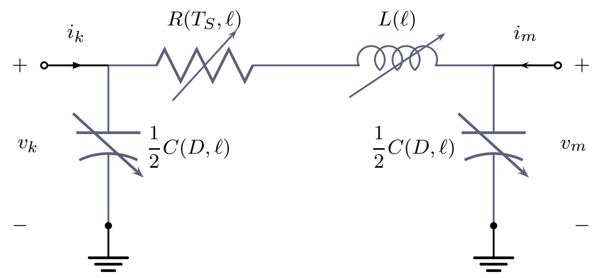

Fig. 2: Mechanical and thermal variables that influenced *RLC* parameters of an OHL modelled by π equivalent circuit

$$\frac{EA\left(r_s m_c g\right)^2}{24} = H^2\left[H - H_{T_{ref}} + \frac{EA\left(r_s m_c g\right)^2}{24 H_{T_{ref}}{}^2} + EA\varepsilon_t\left(T_S - T_{ref}\right)\right] \tag{2}$$

Equation (2) relates the tension H_S at a temperature T_S by means of a known H_{Tref} at a known temperature T_{ref}, where E is the modulus of elasticity of the conductor, A is the conductor cross section, g is the gravitational constant, m_c is the conductor mass per unit length, r_s is the equivalent ruling span length, and ε_t is the coefficient of thermal expansion. ε_t is a function of the stress and the elastic modulus. This dependence has a considerable influence at high temperatures [21], however in this research it is assumed constant, because the temperatures assumed in the simulations are below of 25 °C. Finally, as the values of H_{Tref} and ε_t vary over time, a continuous estimation of these value is necessary.

The conductor length per phase (ℓ) can be computed using OHL geometry and tension (H) by means of

$$\ell = \sqrt{h^2 + \left[\frac{2H}{m_c g}\sinh\left(\frac{m_c g s}{2H}\right)\right]^2} \tag{3}$$

where h is the vertical distance between support elevation points (inclined spans) and s is the span length.

Finally, the OHL sag (D) is computed by

$$D = \frac{H}{m_c g}\left[\cosh\left(\frac{m_c g s}{2H}\right) - 1\right] \tag{4}$$

2.3 *Electro-Magnetic phenomena*

The electrical parameters of the π equivalent circuit (fig. 2) by which the Electro-Magnetic phenomena can describe are used for modelling OHLs with medium length. These parameters are influenced by variations both in load and weather as follows

The equivalent conductor resistance (R) varies according to temperature (T_S) and conductor length (ℓ). These variations can describe by

$$R_{T_S} = R_{T_{ref}}\left(1 + \alpha\left(T_S - T_{ref}\right)\right) \cdot \frac{\ell_{T_S}}{\ell_{T_{ref}}} \tag{5}$$

where α is the resistance temperature coefficient. This equation is valid as long as the conductivity of material is in the linear zone regarding temperature dependence, which occurs in the normal operation of OHLs.

The equivalent inductance (L) depends on conductor's arrangement, distances among them, and length of phase conductor. This parameter can be computed using

$$L = 2 \cdot 10^{-4} \ln\left(\frac{GMD}{GMR}\right) \cdot \ell \tag{6}$$

where GMD is the geometric mean distance and GMR is the geometric mean radius.

The length of phase conductor and the average distance (h_{avg}) between conductor and ground influences the equivalent capacitance (C). To calculate C from geometry, eq. (7) can use [5],

$$C = \frac{0.05556 \cdot 10^{-6}}{\ln\left(k_1 \dfrac{GMD}{GMR_c}\right)} \cdot \ell \tag{7}$$

where k_1 depends on h_{avg}. Reference [22] uses (8) for computing h_{avg},

$$h_{avg} = \frac{\sqrt{(2h_M - D_{avg})\, D_{avg}}}{\log\left(\dfrac{h_M + \sqrt{(2h_M - D_{avg})\, D_{avg}}}{h_M - D_{avg}}\right)} \tag{8}$$

where D_{avg} is the average sag and h_M is the conductor height at the tower. This expression takes into account sag variation which is function of temperature.

3 Error Propagation

In this paper, expressions to compute error propagation are proposed, provided that PMU measurements are used to estimate conductor temperature.

The sensibility on the computation of temperature using resistance is given by influence of the coefficient α as follows

$$T_S = \frac{1}{\alpha}\left(\frac{R'_{T_S}}{R'_{T_{ref}}} - 1\right) + T_{ref} \tag{9}$$

Thus, the error propagates according to

$$\sigma_{T_S} = \frac{dT_S}{dR'_{T_S}}\sigma_R = \frac{1}{\alpha R'_{T_{ref}}}\sigma_R \tag{10}$$

The value of σ_R depends on the devices accuracy as well as load and impedance of OHL. The impact of load in the estimation of temperature is explained by means of an error propagation on the measurements. To carry out this analysis, it is assumed that influence of the OHL capacitance is negligible, obtaining

$$R \approx \mathrm{Re}\left(\frac{v_k - v_m}{i_{km}}\right) \tag{11}$$

Thus, the uncertainty is propagated according to

$$\begin{aligned}
\sigma_R &= \sqrt{\left(\frac{\partial R}{\partial v_k}\sigma_v\right)^2 + \left(\frac{\partial R}{\partial v_m}\sigma_v\right)^2 + \left(\frac{\partial R}{\partial i_{km}}\sigma_{i_{km}}\right)^2} \\
\frac{\partial R}{\partial v_k} &= \frac{\cos\left(\angle v_k - \angle i_{km}\right)}{|i_{km}|} \\
\frac{\partial R}{\partial v_m} &= -\frac{\cos\left(\angle v_m - \angle i_{km}\right)}{|i_{km}|} \\
\frac{\partial R}{\partial i_{km}} &= \frac{|v_k|\cos\left(\angle v_k - \angle i_{km}\right) - |v_m|\cos\left(\angle v_m - \angle i_{km}\right)}{|i_{km}|^2}
\end{aligned} \tag{12}$$

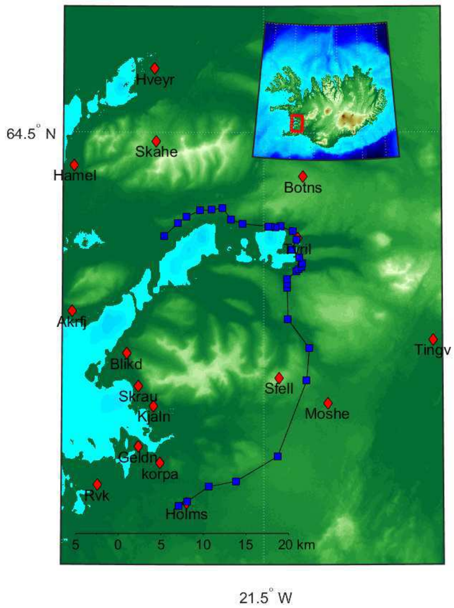

Fig. 3: Geographic location of BR1-OHL ruling spans (blue squares) and nearby weather stations (red diamonds)

4 Case Study

To analyse the impact of both weather and PMU measurement errors in the estimation of OHL's RLC parameters and conductor temperature, this paper studies the OHL identified as BR1 that belongs to the Icelandic transmission system operated by Landsnet. This OHL connects geothermal plants and the substation Brennimelur, and it is considered as the most critical connection in the country [23]. As shown in fig. 3, BR1 connection crosses mountains, valleys and the sea, and it was built with three different types of conductors; therefore, temperature variations along the conductor occur. Given these characteristics, DLR is an option to increase the reliability and capacity of BR1-OHL.

4.1 Test Line

BR1 has a rate voltage of 220 [kV], a length of 59.4 [km] and it is suspended at 172 towers divided in 30 tension sections shown in table 1. In this work, each stringing section is approached to a ruling span [21]. Different types of conductors are used on the OHL; their properties are shown in table 2. Weather conditions for static rating are: ambient temperature $T_a = 10\,[^\circ\mathrm{C}]$, wind speed and attack angle $\vec{\vartheta}_a = 0.6\angle 90^\circ\ [\mathrm{m/s}]$ and solar radiation $S = 0\,[\mathrm{W/m^2}]$ for an allowable conductor temperature $T_S = 40\,[^\circ\mathrm{C}]$.

4.2 Weather Nowcasting

To compute conductor temperature in each ruling span, this work assumes that atmospheric conditions do not change along each ruling span. Thus, atmospheric conditions were interpolated through biharmonic splines, evaluating the points located in the middle of each ruling span using records and location of weather station and the function *griddata* of Matlab®. An accurate model of weather nowcasting is beyond the scope of this paper, because of this work only seeks to analyse the influence of weather variations as well as PMU measurement errors on estimation of conductor capacity. There are sixteen weather stations close to BR1-OHL; their names and locations are shown in table 3. The measure records from these stations are available online at the Islandic Met Office webpage. For DLR, it is recommended to take 10 or 15 min average and standard deviation of samples [24]. However, as the aim of this paper is to evaluate the performance to use PMU for DLR, the atmospheric conditions between *2016-04-18 00:00* and *2016-04-18 21:00*, with

Table 1 BR1 OHL - Stringing sections characteristics

Ruling Span	Conductor Type	Capacity [MVA]	Spans Length [m]
1	470-AL3	304	289 387 440
2	470-AL3	304	230 395 302 308 392 410 337 336 359
3	470-AL3	304	436 398 457 340 277 188 432 268 187 331
4	470-AL3	304	421 343 394 408 308 397 414 313 376 435 435 436 405 208 394
5	470-AL3	304	318 449 386 414 386 441 413 402 441 410 416 433 405 431 395 444 408 428 391 367 353 342 349 375
6	470-AL3	304	379 453 317 299 411 328 450 418 416 308
7	470-AL3	304	388 389 446 429 433 293 377 446 372 446 225
8	470-AL3	304	387 389 294 224 241 455 272 398 414 366 398 354 252
9	470-AL3	304	426
10	470-AL3	304	197 213 194
11	470-AL3	304	208 140 136 183 162 136 142 146 133
12	470-AL3	304	400
13	470-AL3	304	392
14	470-AL3	304	480
15	470-AL3	304	272 295 192
16	6469-AL3134ST4A	304	202 909 159
17	470-AL3	304	318 278 371 329
18	470-AL3	352	316 316 233 217
19	470-AL3	304	258 383 327 374 255
20	470-AL3	304	377 182
21	470-AL3	304	270 284
22	470-AL3	304	312
23	470-AL3	304	380 290 362 378 388 349 303 280 341
24	470-AL3	304	373 329 365 347
25	774-AL3	304	468 329 289 580
26	2X774-AL3	415	222 349 337 387
27	2X774-AL3	830	441 249 288 349
28	2X774-AL3	830	193 398 307 238 351 316
29	2X774-AL3	830	173 260 276 213 297
30	2X774-AL3	830	368 384 398 385 337 340

Table 2 BR1 OHL Conductors

	470-AL3	6469-AL3 /134ST4A	774-AL3	unit
Type	$ACAR$	$ACSR$	$ACAR$	
A	469.6×10^{-6}	469×10^{-6}	774.2×10^{-6}	m^2
m_c	1.294	2.4217	2.140	$\mathrm{kg/m}$
E	57000×10^6	67100×10^6	55000×10^6	$\mathrm{N/m}^2$
ε_t	23×10^{-6}	19.3×10^{-6}	23×10^{-6}	$1/\mathrm{K}$
$R'_{T_{ref}}$	0.07415×10^{-3}	0.0768×10^{-3}	0.0389×10^{-3}	Ω/m
α	0.0036	0.0038	0.0036	$1/\mathrm{K}$
T_{ref}	25	20	20	$^\circ\mathrm{C}$
α_s	0.5	0.5	0.5	1
ε	0.5	0.5	0.5	1
d	28.14×10^{-3}	32.28×10^{-3}	36.18×10^{-3}	m

samples taken every three hours, were considered. As example, temperature and wind interpolations for the date *2016-04-18 21:00* are shown in fig. 4. Given the climate characteristics of Iceland, solar radiation is neglected [23] and normally the Icelandic Met Office does not report this parameter.

5 Impact of atmospheric variations

To analyse the impact of atmospheric variations on the BR1-OHL capacity, thermal, mechanical and electrical variables were calculated for each ruling span using weather interpolation and OHL geometry. Figure 5 shows the flowchart for computing the values of these variables (T_S, ℓ, S, H, R, L, C). Afterwards, in order to evaluate PMU performance, these results are compared with the values computed using synchrophasors simulations. These simulations are assumed at the ends of the OHL. Thus, with the phasor simulations of v_k, i_k, v_m, i_m and with (13) and (14), the average temperature T_S is computed through the estimation of circuit parameters of fig. 2.

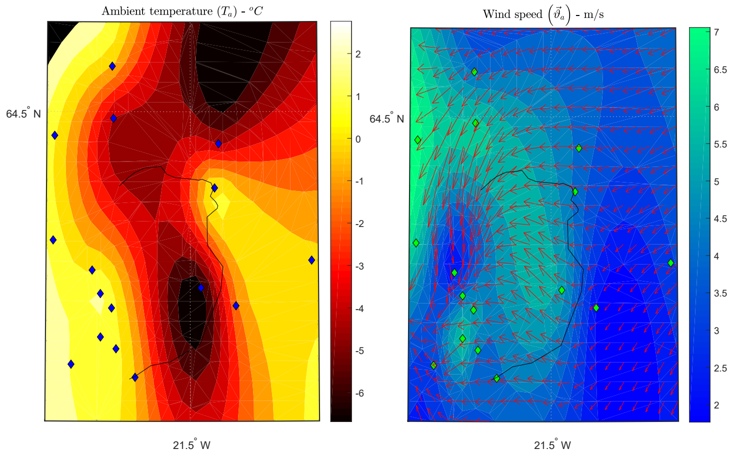

Fig. 4: Weather nowcasting for the area of influence of BR1 OHL, at *2016-04-18 21:00*
a Temperature
b Wind speed

Table 3 Weather station close to the *BR1* influence area

Weather station	WMO number	Latitude [°]	Longitude [°]
Rvk	04030	64.1275	-21.9028
Holms	04920	64.1085	-21.6864
Korpa	04132	64.15049	-21.75109
Geldn	04880	64.1678	-21.8038
Kjaln	04848	64.2106	-21.7667
Skrau	04818	64.2318	-21.8046
Blikd	04912	64.2664	-21.8329
Sfell	04136	64.2405	-21.4633
Moshe	04918	64.214	-21.3448
Tingv	04142	64.2807	-21.0875
Akrfj	04926	64.3105	-21.966
Tyril	04806	64.3877	-21.4169
Botns	04814	64.4529	-21.4034
Skahe	04904	64.4902	-21.7621
Hamel	04128	64.4647	-21.9628
Hveyr	04134	64.567	-21.767

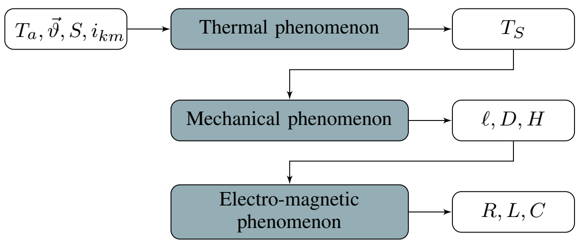

Fig. 5: Flowchart to compute each OHL parameter which vary with the weather and current intensity

$$Z = \frac{{v_k}^2 - {v_m}^2}{v_m i_k - v_k i_m} \tag{13}$$

$$Y = \mathrm{Im}\left(2 \cdot \frac{i_k + i_m}{v_k + v_m}\right) \tag{14}$$

The current intensity i_{km} used to compute the OHL parameters is given by

$$i_{km} = i_k - \frac{v_k Y}{2} \tag{15}$$

PMU values were simulated with SIMULINK® as follows: a power flow for circuit of fig. 2 is run initially assuming design values of resistance, inductance and capacitance under rate conditions,

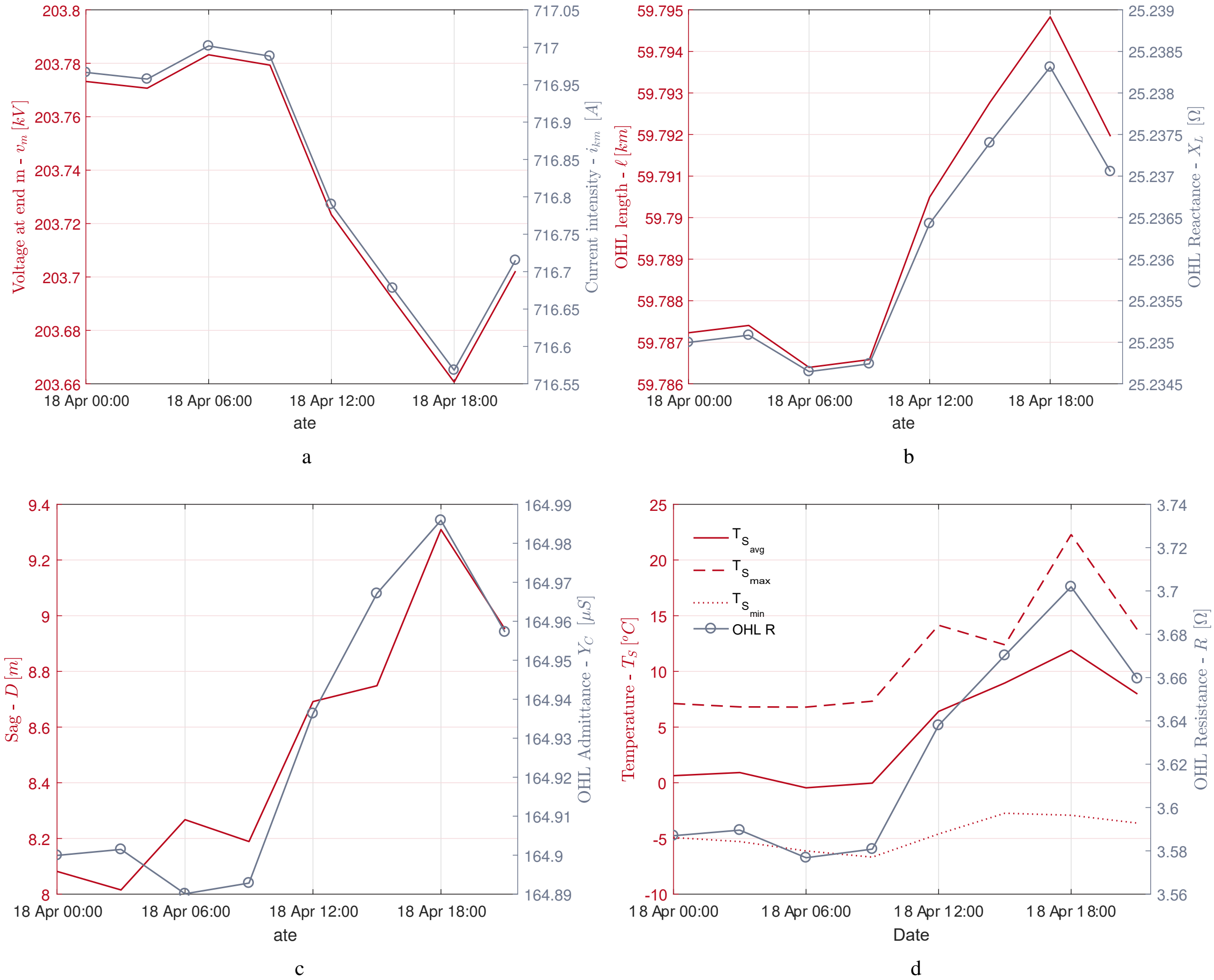

Fig. 6: Variation of the parameters of the BR1-OHL for each weather sample
a Current intensity (i_{km}) flowing through the OHL and voltage at end m (v_m)
b Inductance (reactance) and phase conductor length
c Capacitance (admittance) and sag of ruling span number 8
d Resistance, average temperature and, maximum and minimum temperature along the OHL

$v_k = 220\,[\text{kV}]$, $S = 304\,[\text{MVA}]$ and $PF = 0.9$. Afterwards, an iterative script was implemented changing the RLC values of π model according to (5), (6) and (7), with the aim of updating the electrical parameters considering the changes in conductor temperature. This script runs until the current intensity computed through the load flow is equal to the current i_{km} used for calculating the resistance from (5). As simulations results, fig. 6 shows variations of the ℓ, X_L, Y_C, R, D and T_S parameters for each weather sample. These values are of the entire OHL except D which is the sag of the ruling span number 8. This span was chosen because of it has the highest variation within samples, approx. $1.3\,[\text{m}]$. Thus, weather influence over the sag can be determined.

In fig. 6a are shown the values both of current intensity i_{km} and of voltage v_m obtained for each sample. The maximum variation of the entire phase conductor length is less than 0.02%, which corresponds to $9\,[\text{m}]$. This means that the OHL inductance is not affected as a consequence of typical atmospheric variations. Therefore, the phase conductor length can assume constant, as shown in fig. 6b. In the same way, the variation between the maximum and minimum value of the equivalent capacitance is less than 0.2%, making negligible the influence of the sag (D), as shown in fig. 6c. On other hand, the resistance changes up to 3.5%, as shown in fig. 6d. In this fig., the average conductor temperature $\left(T_{S_{avg}}\right)$ is computed using the resistance, obtaining a maximum and minimum of $6.7\,[^{\circ}\text{C}]$ and $2.6\,[^{\circ}\text{C}]$, respectively. In all samples, the differences between $T_{S_{avg}}$ and $T_{S_{max}}$ exceed the acceptable error margin for critical spans of $4\,[\text{K}]$ $(10\%$ of $40\,[^{\circ}\text{C}])$ proposed in [6]. The maximum temperature $\left(T_{S_{max}}\right)$ and minimum temperature $\left(T_{S_{min}}\right)$ were obtained by computing the temperature from weather in all ruling spans and taking the highest and lowest of these values.

As a consequence of using different conductors in BR1-OHL, the value of T_S in each ruling span varies, even if the weather does not change along it. In this work, this is considered by using the following procedure: an equivalent temperature $\left(T_{S_{avg}}\right)$ is computed with (16) using the resistance $\left(R_{equiv}\right)$ calculated with (5).

$$T_{S_{avg}} = \frac{R_{equiv} - \sum_{i=1}^{N} R_i\left(T_{ref}\right) + \sum_{i=1}^{N} R_i\left(T_{ref}\right)\cdot\alpha_i\cdot T_{ref}}{\sum_{i=1}^{N} R_i\left(T_{ref}\right)\cdot\alpha_i} \tag{16}$$

With this equivalent temperature and supposing initial values of average ambient temperature $(T_{a_{k=0}})$ and solar radiation, an equivalent cooling heat is computed. With this parameter, an equivalent wind speed $\left(\vec{\vartheta}_{equiv}\right)$ is calculated [25] along entire OHL. With these new atmospheric conditions, the temperature in each ruling span (T_{S_i}) is calculated, thus the resistivity of each conductor is considered. However, as T_a is originally guessed, it is necessary to adjust this value via iterations until the difference between the

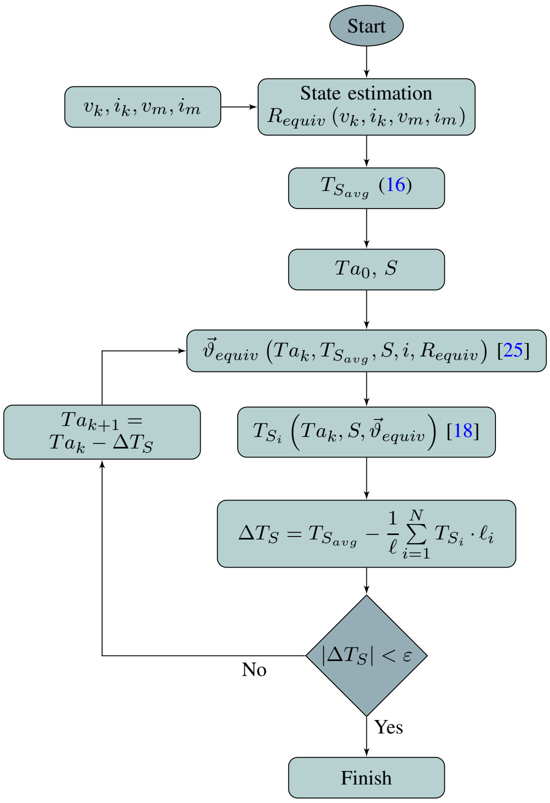

Fig. 7: Flow chart for computing T_S in each ruling span using PMU measurements

weighted average of $\left(T_{S_i}\right)$ and $\left(T_{S_{avg}}\right)$ is less than an error (ε). This procedure is shown in fig. 7.

Figure 8 shows both the temperature and the error calculated with the atmospheric conditions in each ruling span and the temperature computed using simulations of PMU measurements. Figure 8a shows a dynamic behaviour in time and space (along the OHL) of the conductor temperature. Moreover, the critical ruling span changes for each weather sample, and the acceptable error margin of $(4[\mathrm{K}])$ is exceeded between the different critical spans, as shown in fig. 8b. The critical span was assumed as the span with the highest temperature.

6 PMU Measurement Error Impact

6.1 *Impact on the accuracy*

In this section, conductor's temperature is estimated considering errors in PMU measurements. Measurement errors were simulated assuming a random normal distribution of error with mean zero and standard deviation approximated to $1/3$ of meter accuracy. A typical accuracy of 0.3% was assumed for measurement simulations for both current and voltage [26]. The angle between phasors was taken without error; this is analysed in [27]. Additionally, the estimation algorithm proposed in [10] was implemented in order to reduce the error in the computing of OHL resistance and average conductor temperature.

For each weather sample, $1,000$ simulations were run by adding normal random errors to PMU measurements of v_k, i_k, v_m, i_m. Random errors were simulated with Matlab®. Figure 9a shows the measurement error impact on the resistance estimation, obtaining an uncertainty of approximately 16 %. The uncertainty in this work is assumed as three times the standard deviation (σ). This uncertainty is equivalent to an error within $\pm 0.6\,[\Omega]$, considering a normal distribution with a mean between $3.6\,[\Omega]$ and $3.7\,[\Omega]$. Thus, the error in the estimation of the equivalent resistance per unit length $\left(R'_{eqv}\right)$ is within $\pm 10 \times 10^{-3}\,[\Omega/\mathrm{km}]$. This error propagates to the computing of temperature, reaching errors within $\pm 38\,[\mathrm{K}]$, as shown in fig. 9b.

In the case studies, the 470-AL3, 6469-AL3 /134ST4A and 774-AL3 conductors, which are used in BR1-OHL, the errors calculated by (10) are within $\pm 37\,[\mathrm{K}]$, $\pm 34\,[\mathrm{K}]$ and $\pm 36\,[\mathrm{K}]$, respectively. These values are close to the values shown in fig. 9b. The differences are due to the use of R'_{equiv} for computing the standard deviation σ_r.

6.2 *Impact of load on the estimation of conductor temperature*

As voltage and current magnitudes depend on load and OHL impedance, the latter influence the resistance estimation, and therefore, the computing of conductor temperature. A simulation like the one of the previous section is carried out for the weather sample 2016-04-18 21:00, changing the load between 0.1 and 1 [pu] and the power factor (PF) between 0.1 and 0.95 . The simulation results are shown in fig. 10. The standard deviation σ was calculated with the 500 runs for each set of loads and PFs. In the estimation of the equivalent resistance $\left(R_{equiv}\right)$ and the computing of conductor temperature T_S, the minimum standard deviation was $0.027\,[\Omega]$ and $1.9\,[\mathrm{K}]$, respectively, for a power factor of 0.1 and a load of 1 [pu]. The maximum standard deviation was $2.41\,[\Omega]$ and $172\,[\mathrm{K}]$ for a power factor of 0.95 and a load of 0.1 [pu].

Given that $\sigma_R \propto 1/i_{km}$ in (10), the uncertainty in the computing of temperature is increased at low power flows. Additionally, if the power factor (*PF*) is approximated to $\cos \angle i_{km}$ (using $\angle v_k = 0$ as reference, $\angle v_m$ close to $\angle v_k$ and $\angle i_{km}$ measured with respect to $\angle v_k$) the uncertainty increases as PF is close to 1. On the other hand, typical ratio between magnitudes of voltage (kV) and current (A) in power transmission systems impacts the measurement error in resistance computing.

The simulation results of this paper were not contrasted with real PMU's measurements at the same time. However, reference [2] reports results about the use of PMU measurements in the studied BR1-OHL. The temperature obtained was outside the acceptable error margins. Additionally, reference [28] reports high variation including negative values in the computation of the resistance in a real OHL when PMU measurements are used. Both results are consistent to those obtained in this paper. Therefore, using the proposed methodology, the PMU performance could be predicted.

7 Discussion

Based on both the weather variations along OHLs and error in PMU measurements, a methodology to assess the use of synchrophasors as DLR method was introduced. Its main advantage is to use simulations and expressions to evaluate the performance of PMU for DLR during the planning stage. For instance, as a result of using this methodology in the case study in this paper, the BR1-OHL capacity cannot be estimated using PMU. Thus, applying this methodology would reduce costs by avoiding future fail implementations. However, provided that a successful result of applying the proposed methodology is achieved, further analysis and validation must be carried out before implementing PMU as DLR method. This analysis should include the presence of uncorrelated data as well as bad data and a more accurate model to describe stringing sections given the limitation of ruling span approximation, mainly at high operating temperatures.

8 Conclusions

The changes in the load and the atmospheric conditions along an OHL result in alteration of thermal and mechanical variables, which affect the electrical RLC parameters. This influence is negligible for inductance and capacitance under typical atmospheric and load conditions, as a consequence of the small variation of the line length and

IET Research Journals, pp. 1–9

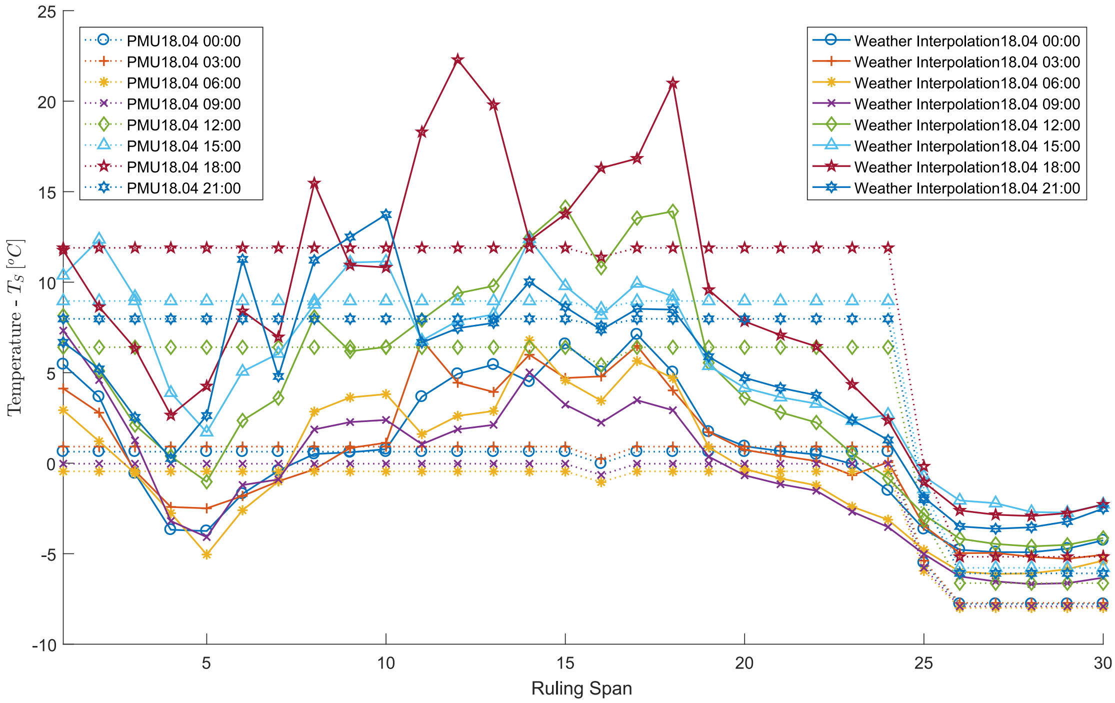

a

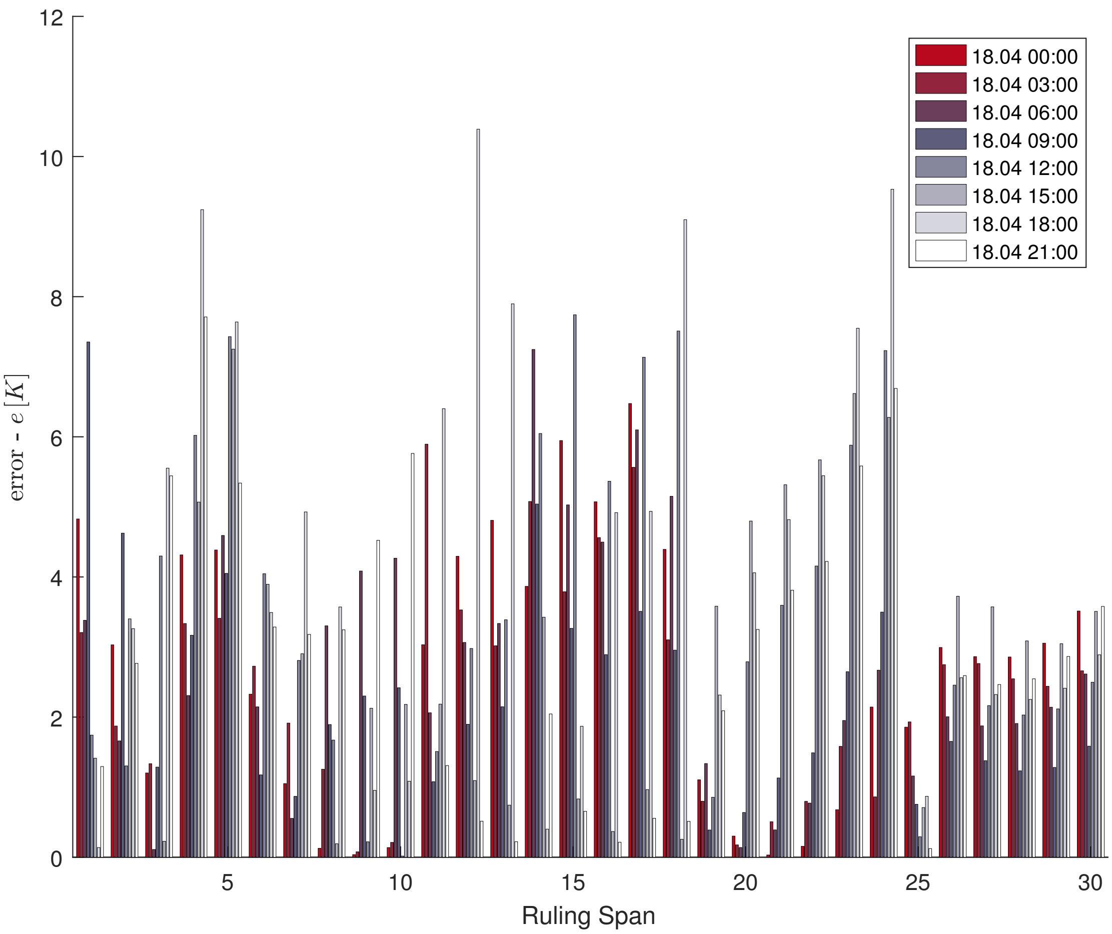

b

Fig. 8: Comparison between temperatures computed using weather interpolation and using PMU estimation in each ruling span for different times
a Temperature of the conductor - T_S
b Error between T_S computed using weather interpolation and PMU estimation

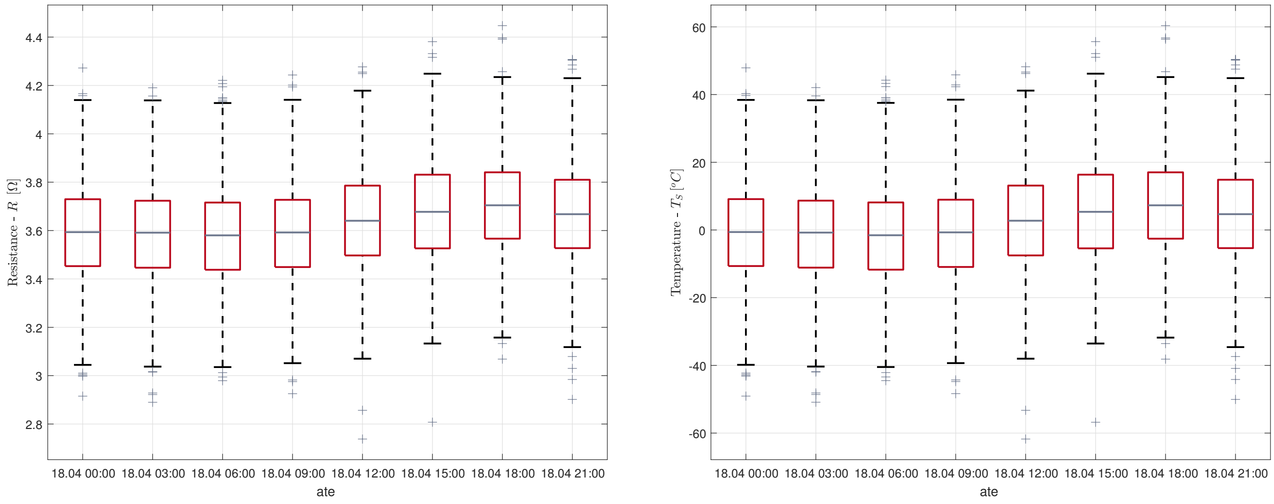

a

b

Fig. 9: Box plots with the value of both OHL resistance and $T_{S_{avg}}$ estimated using PMU for each sample, assuming an accuracy of 0.3% in simulations of voltage and current measurements
a OHL resistance
b Average temperature of the conductor -$T_{S_{avg}}$

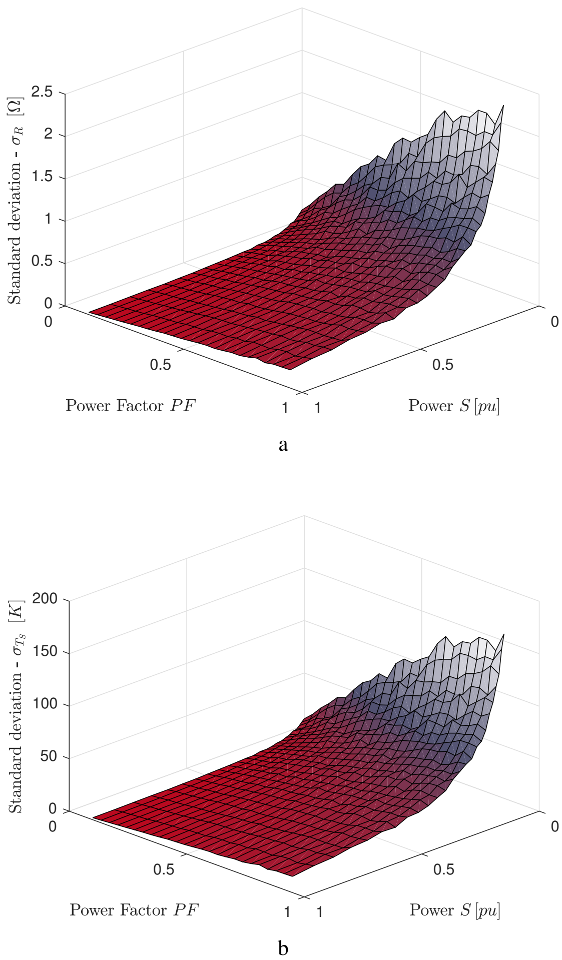

Fig. 10: Influence of load on the estimation of both conductor's resistance and temperature using PMU measurements
a OHL's resistance
b Average conductor temperature -$T_{S_{avg}}$

low impact of the sag on the capacitance. On the contrary, the value of the resistance changes in a non-neglected way.

The use of PMU's measurements for DLR faces challenges when atmospheric conditions and conductor properties change along OHLs, together with inaccuracy, due to the error propagation in the computation of resistance. Thus, the average value of temperature computed from PMU measurements could not depict the real conductor capacity and jeopardizes OHL, as shown in this paper. This as a consequence of exceeding accepted security margins in critical spans if the temperature computed with synchrophasors are used. Additionally, the estimated conductor's temperature error can be outside acceptable margins, as a result of the sensibility of temperature with resistance, even if state estimation algorithms are used. For these reasons, a methodology to asset the use of PMU for DLR is proposed. As future research, error minimization techniques that account weather models, PMU and the monitoring of critical spans could potentially improve the estimation of conductor rating.

Acknowledgment

Authors thank LANDSNET-Iceland, for providing the test cases in section 4. This research was supported by the Colombian Department of Science, Technology and Innovation (Colciencias) under the project 617 - National Doctorates.

9 References

1 Winter, W., Elkington, K., Bareux, G., Kostevc, J.: 'Pushing the Limits: Europe's New Grid: Innovative Tools to Combat Transmission Bottlenecks and Reduced Inertia', *IEEE Power and Energy Magazine*, 2015, **13**, (1), pp. 60–74. Available from: http://ieeexplore.ieee.org/document/6998972/
2 Sun, W.Q., Zhang, Y., Wang, C.M., Song, P.: 'Flexible load shedding strategy considering real-time dynamic thermal line rating', *Generation, Transmission Distribution, IET*, 2013, **7**, (2), pp. 130–137. Available from: http://ieeexplore.ieee.org/document/6519364/
3 CIGRE WG B2. 13. 'Guidelines for increased Utilization of existing Overhead Transmission Lines'. Technical Brochure 353. (Paris: CIGRE, 2008.
4 Douglass, D., Chisholm, W., Davidson, G., Grant, I., Lindsey, K., Lancaster, M., et al.: 'Real-Time Overhead Transmission-Line Monitoring for Dynamic Rating', *IEEE Transactions on Power Delivery*, 2016, **31**, (3), pp. 921–927. Available from: http://ieeexplore.ieee.org/document/6991585/
5 Papailiou, K.O.: 'Overhead Lines: A Cigre Green Book'. (Cigre, 2014)
6 CIGRE WG B2. 36. 'Guide for Application of Direct Real-Time Monitoring Systems'. Technical Brochure 498. (Paris: CIGRE, 2012.
7 International des grands réseaux électriques. Joint working group B2-C1 (19), C.: 'Increasing Capacity of Overhead Transmission Lines: Needs and Solutions'. (CIGRE, 2010). Available from: http://www.e-cigre.org/

8 Fernandez, E., Albizu, I., Bedialauneta, M.T., Mazon, A.J., Leite, P.T.: 'Review of dynamic line rating systems for wind power integration', *Renewable and Sustainable Energy Reviews*, 2016, **53**, pp. 80–92
9 Alvarez, D.L., Rosero, J.A., Faria da Silva, F., Bak, C.L., Mombello, E.E. 'Dynamic line rating — Technologies and challenges of PMU on overhead lines: A survey'. In: 2016 51st International Universities Power Engineering Conference (UPEC). (Coimbra: IEEE, 2016. pp. 1–6. Available from: http://ieeexplore.ieee.org/document/8114069/
10 Du, Y., Liao, Y.: 'On-line estimation of transmission line parameters, temperature and sag using PMU measurements', *Electric Power Systems Research*, 2012, **93**, pp. 39–45
11 Rehtanz, C.: 'Synchrophasor based thermal overhead line monitoring considering line spans and thermal transients', *IET Generation, Transmission & Distribution*, 2016, **10**, (5), pp. 1232–1239(7)
12 Bockarjova, M., Andersson, G. 'Transmission Line Conductor Temperature Impact on State Estimation Accuracy'. In: 2007 IEEE Lausanne Power Tech. (IEEE, 2007. pp. 701–706. Available from: http://ieeexplore.ieee.org/lpdocs/epic03/wrapper.htm?arnumber=4538401
13 Frank, S., Sexauer, J., Mohagheghi, S.: 'Temperature-Dependent Power Flow', *IEEE Transactions on Power Systems*, 2013, **28**, (4), pp. 4007–4018
14 Sivanagaraju, G., Chakrabarti, S., Srivastava, S.C.: 'Uncertainty in Transmission Line Parameters: Estimation and Impact on Line Current Differential Protection', *Instrumentation and Measurement, IEEE Transactions on*, 2013, **PP**, (99), pp. 1
15 Cecchi, V., Leger, A.S., Miu, K., Nwankpa, C.O.: 'Incorporating Temperature Variations Into Transmission-Line Models', *IEEE Transactions on Power Delivery*, 2011, **26**, (4), pp. 2189–2196
16 Matus, M., Saez, D., Favley, M., Suazo.Martinez, C., Moya, J., Jimenez.Estevez, G., et al.: 'Identification of Critical Spans for Monitoring Systems in Dynamic Thermal Rating', *IEEE Transactions on Power Delivery*, 2012, **27**, (2), pp. 1002–1009. Available from: http://ieeexplore.ieee.org/document/6163401/
17 Mai, R., Fu, L., HaiBo, X. 'Dynamic Line Rating estimator with synchronized phasor measurement'. In: 2011 International Conference on Advanced Power System Automation and Protection. vol. 2. (IEEE, 2011. pp. 940–945. Available from: http://ieeexplore.ieee.org/document/6180545/
18 Stephen, R., Douglas, D., Mirosevic, G., Argasinska, H., Bakic, K., Hoffman, S., et al.: 'Thermal behaviour of overhead conductors'. (CIGRE, 2002). Available from: http://www.e-cigre.org/
19 IEEE Std 738-2006: 'IEEE Standard for Calculating the Current-Temperature of Bare Overhead Conductors'. (, 2007)
20 Motlis, Y., Barrett, J.S., Davidson, G.A., Douglass, D.A., Hall, P.A., Reding, J.L., et al.: 'Limitations of the ruling span method for overhead line conductors at high operating temperatures', *IEEE Transactions on Power Delivery*, 1999, **14**, (2), pp. 549–560. Available from: http://ieeexplore.ieee.org/document/754102/
21 CIGRE TF B2. 12. 3. 'Sag-Tension calculation methods for overhead lines'. Technical Brochure 324. (Paris: CIGRE, 2007. p. 91
22 Tleis, N.: 'Power Systems Modelling and Fault Analysis: Theory and Practice'. Newnes Power Engineering Series. (Elsevier Science, 2007)
23 Jiliusson, S.R. 'Using PMU Measurements to Assess Dynamic Line Rating of Transmission Lines' [M.Sc. Thesis in Electrical Power Systems and High Voltage Engineering]. Aalborg University, 2013. Available from: http://projekter.aau.dk/projekter/files/77194901/Dynamic_Line_Rating.pdf
24 CIGRE WG B2. 12. 'Guide for Selection of Weather Parameters for Bare Overhead Conductor Ratings'. Technical Brochure 299. (Paris: CIGRE, 2006.
25 Albizu, I., Fernandez, E., Eguia, P., Torres, E., Mazon, A.J.: 'Tension and Ampacity Monitoring System for Overhead Lines', *IEEE Transactions on Power Delivery*, 2013, **28**, (1), pp. 3–10. Available from: http://ieeexplore.ieee.org/document/6313952/
26 IEEE Std C57. 13-2016: 'IEEE Standard Requirements for Instrument Transformers', *IEEE Std C5713-2016 (Revision of IEEE Std C5713-2008)*, 2016, pp. 1–96
27 Zhao, J., Tan, J., Wu, L., Zhan, L., Liu, Y., Gracia, J., et al.. 'Impact of Measurement Error on Synchrophasor Applications'. (, 2015. Available from: https://certs.lbl.gov/publications/impact-measurement-error
28 Carlini, E.M., Pisani, C., Vaccaro, A., Villacci, D. 'Dynamic Line Rating monitoring in WAMS: Challenges and practical solutions'. In: 2015 IEEE 1st International Forum on Research and Technologies for Society and Industry, RTSI 2015 - Proceedings. (IEEE, 2015. pp. 359–364